Compliance-Based Dynamic Steering for Hexapods

David Zarrouk[1], Ronald S. Fearing[2]

***Abstract*—This paper proposes a novel dynamic gait of locomotion for hexapedal robots which enables them to crawl forward, backward, and rotate using a single actuator. The gait exploits the compliance difference between the two sides of the tripods, to generate clockwise or counter clockwise rotation by controlling the acceleration of the robot. The direction of turning depends on the configuration of the legs -tripod left of right- and the direction of the acceleration. Alternating acceleration in successive steps allows for continuous rotation in the desired direction. An analysis of the locomotion is presented as a function of the mechanical properties of the robot and the contact with the surface. A numerical simulation was performed for various conditions of locomotion. The results of the simulation and analysis were compared and found to be in excellent match.**

I. INTRODUCTION

Much of the interest in insect-like locomotion has been motivated by the need for low cost, small, fast, and robust robots capable of crawling on a variety of rough terrains. This will enable them to reach remote areas inaccessible for humans or wheeled vehicles, for inspection, reconnaissance or search and rescue.

Several research groups invested considerable effort in investigating hexapedal robots producing numerous designs, some of which are capable of running at more than ten body lengths per second such as Mini-Whegs [10], Dyna-RoACH [5], DASH [1] and iSprawl [8]. Phasing between the legs can be achieved using controllers [10] [8], or mechanically [5] [1]. Various steering mechanisms were also suggested; RHex [15] and OctoRoACH [11] rely on differential velocity drive, Sprawlita [2] and iSprawl [8] [9] actively change their leg kinematics, and OctoRoACH [11] can be steered using a dynamic tail.

Schmitt and Holmes [12] [13] and Kukillaya and Holmes [7] investigated the dynamic model of cockroaches. They limited their analysis to plane dynamics and modeled the legs as two rigid links connected to each other and to the main body through an active torsional spring. Stability of the locomotion [4] together with the response to quick perturbations [3] were also considered. The influence of compliant contact (foot and/or surface) on crawling was investigated by Zarrouk et al. [16][17] who studied the locomotion of worm robots and formulated the locomotion efficiency as a function of the compliance, coefficient of friction (COF), and external forces.

Inspired by cockroach locomotion and the influence of compliance on the velocity of the robot, this paper shall present a new gait which enables operating a robot in a plane using a single actuator/motor. The gait control exploits the disparity in stiffness between the two sides of the tripod (the stiffness of two legs versus one leg), which together with inertial forces induced by acceleration, generate different progress of the two sides of the robot. Controlled successive tilting, together with proper phasing in consecutive steps, produces yaw rotation in a desired direction.

Towards this goal, we first formulate a static and dynamic model of the robot. The model is used to obtain a preliminary estimate of the motion, as a function of the robot properties and actuation parameters, and to perform a numerical simulation.

To validate our analysis, we developed a numerical simulation based on realistic parameters obtained from previous work [5] [1]. The simulation allows us to first validate our results and second, to find optimum parameters for robot design and optimum control parameter for good stability and performance.

II. SYSTEM DEFINITION

A. General description of the robot model

We consider a hexapedal robot consisting of a main body and six actuated flexible legs which rotate around their hips providing thrust (see Figure 1). Similarly to insects, the robot runs with an alternating tripod gait consisting of a left tripod (LT, legs 1,4,5) and a right tripod (RT, legs 2,3,6). A step begins when a tripod contacts the surface and ends when it disengages, marking the beginning of the next step. A cycle is comprised of two successive steps LT and RT.

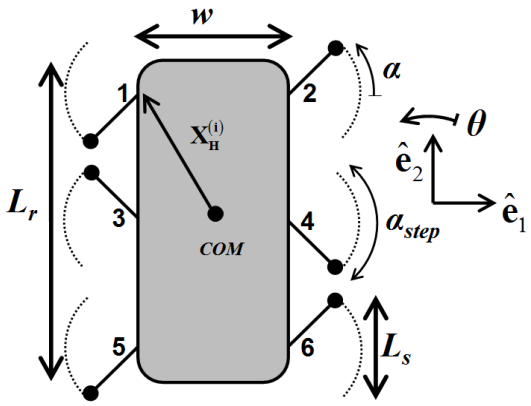

Figure 1 The Hexapod robot. LT is comprised of legs 1,4,5 and RT is made of legs 2,3,6.

We assume that the robot has a rigid body with a mass *m* and inertia moment *I* and that the dynamic model of the robot is restricted to the horizontal plane. The mass of the legs

[1] Department of EECS, UC Berkeley, (zadavid@berkeley.edu)
[2] Department of EECS, UC Berkeley, (Ronf@eecs.berkeley.edu)

constitutes generally a small percentage of total weight and is therefore neglected in this analysis. The center of mass (COM) is the geometrical center of the robot. The legs are rigid against bending but compliant along their length with a spring constant k_l. At their hips, the legs are attached to the motor by a torsional spring whose stiffness is k_r. (see Figure 2).

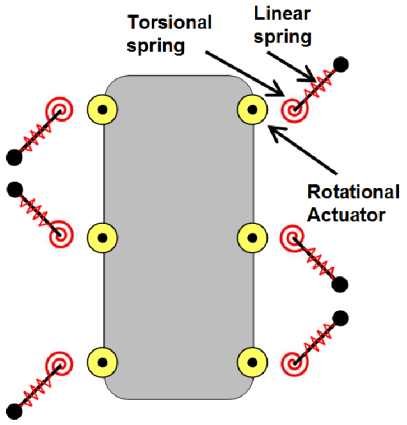

Figure 2. Leg model. Each leg has two elastic DOF, a linear spring along its length and a torsional spring at the hip. The legs rotate around their hips.

The step size, which we denote by L_s, is the distance travelled by the *unloaded* legs relative to the joint of the robot, in parallel to the fore-aft direction.

$$L_s = 2L_0 \cdot \sin\left(\frac{\alpha_{step}}{2}\right) \tag{1}$$

Where L_0 is the length of the leg and α_{step} is the step angle measured from the touchdown of the free legs until disconnecting from the surface. The robot controls the angular velocity of the motors $\dot{\alpha}_{motor}$ (but not that of the legs $\dot{\alpha}_{leg}$). The orientations of the legs and motors are related by

$$\alpha_{leg} = \alpha_{motor} + \Delta\alpha_{spring} \tag{2}$$

where $\Delta\alpha_{spring}$ is the angular deformation of the torsional spring due to load. If the angular velocity of the motor $\dot{\alpha}_{motor}$ is constant, the duration of a step is

$$T_{step} = \frac{\alpha_{step}}{\dot{\alpha}_{motor}} \tag{3}$$

In quasistatic locomotion, the robot advances L_s in a step or $2L_s$ during a cycle. The maximum average velocity of the robot during a step is

$$[V] = 2\frac{\dot{\alpha}_{motor} L}{\alpha_s}\sin\left(\frac{\alpha_s}{2}\right) \tag{4}$$

B. Contact modeling

We assume that at the beginning of a step, the robot places its unloaded legs over the surface with no impact and contacts the surface at their tips only. At the end of the step, the legs detach from the surface and any elastic energy stored in the torsional and linear springs is dissipated. To model the friction between the robot and surface, we adopt the standard physical model of friction, the Coulomb model. The Coulomb model explicitly defines the maximum friction force acting on the tip of the legs as a product of the COF and the normal force.

$$f^{(i)} \le \mu F_n^{(i)} \tag{5}$$

Where $f^{(i)}$ and $F_n^{(i)}$ are respectively the norms of the friction force and normal forces acting on leg i, and μ is the COF. The equality in Eq. (5) holds only when sliding occurs and the friction force direction is opposite to the sliding.

III. STATIC AND DYNAMIC ANALYSIS

In this section we develop the force conditions on the robot, as well as static and dynamic models, which allow us to determine the modes of locomotion of the robot and approximate its linear and angular velocities.

A. Dynamic analysis

The planar forces acting on the robot are the friction forces acting on the tips of the legs and the projection of the weight force along the plane (in case of an incline). Since the legs are assumed massless and their dynamics neglected, the forces acting on the hip joints and the friction forces acting on the tips of the legs are equal. The length of the legs can be calculated as a function of the friction forces and their stiffness

$$L^{(i)} = L_0 + \frac{\mathbf{f}^{(i)} \cdot \mathbf{L}^{(i)}}{k_l L^{(i)}} \tag{6}$$

The bold font stands for vectors. Vector $\mathbf{L}^{(i)}$ is along the length of leg i and its norm $L^{(i)}$ is the length of the leg. The deflection of the torsional spring, due to the moment caused by the friction force, can be calculated using

$$\left|\mathbf{M}^{(i)}\right| = \left|\mathbf{L}^{(i)} \times \mathbf{f}^{(i)}\right| = k_r \Delta\alpha_{spring} \tag{7}$$

The forces $\mathbf{f}^{(i)}$ and moments $\mathbf{M}^{(i)}$ act on the robot at the joints of the legs. The dynamic model of the robot is

$$\mathbf{F} = \sum_i \left(\mathbf{f}^{(i)}\right) + \mathbf{F}_{ext} = m\ddot{\mathbf{X}} \tag{8}$$

where $\mathbf{F}_{ext}$ is an external planar force (weight component for example). The sum of the moments yields the angular acceleration

$$\mathbf{M} = \sum_i \left(\mathbf{X}_H^{(i)} + \mathbf{L}^{(i)}\right) \times \mathbf{f}^{(i)} = I\ddot{\boldsymbol{\theta}} \tag{9}$$

where $\mathbf{X}_H^{(i)}$ is the vector distance between the COM of the robot to the hip of the legs

B Yaw rotation due to stiffness disparity

In Figure 3, the robot is standing on its LT, composed of two left legs and one right leg. If all legs are identical, the stiffness of the left side is roughly double of the stiffness of the right side. However, any force acting on the center of the robot would be distributed almost evenly between the two

sides. The right leg would carry twice as much load as each of the left legs and the deflections will be twice as large.

Figure 4(a) and 4(b), show the robot tilting counter clockwise due to an external force. In case "a", the left side of RT is more compliant and tilts counterclockwise when pushed backward. In case "b", the right side of LT is more compliant and tilts counterclockwise when pulled forward. The mirror cases of "a" and "b", in which the robot turns clockwise, are presented respectively in Figs. 4(c) and 4(d).

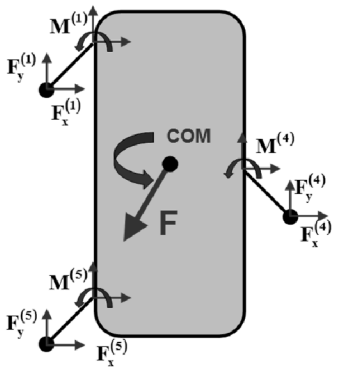

Figure 3. Force diagram of forces acting on the robot during LT configuration.

C. Generating rotation using acceleration

In order to generate successive tilting, and therefore yaw rotation in a desired direction, the robot is accelerated and decelerated in successive steps. To rotate counterclockwise, for example, the robot accelerates in LT configuration (case a) and decelerates during RT configuration (case b). Repetition of the cycle allows for continuous turning. Figure 5 presents the angular velocity profile of the motors. The motor rotates at the angular velocity of $\dot{\alpha}_{motor}$ during the full duration of the first step until reaching the angle $\beta\alpha_{step}$ of the second step. At this point the motor decelerates its velocity to $\gamma\dot{\alpha}_{motor}$ and produces an inertial forward force. At the end of step 2, the robot accelerates back to $\dot{\alpha}_{motor}$ and produces a inertial backward force. While it is practically impossible to generate infinite accelerations, existing miniature robot design show the feasibility of accelerating in roughly one hundredth of a second. The velocity ratio, γ, is confined to the interval [0, 1]. The robot stands still when γ =0 and runs continuously with no accelerations when γ =1. The durations of step 1 and step 2, respectively T_1 and T_2, are

$$T_1 = \frac{\alpha_{step}}{\dot{\alpha}_{motor}} \tag{10}$$

and

$$T_2 = \beta\frac{\alpha_{step}}{\dot{\alpha}_{motor}} + (1-\beta)\frac{\alpha_{step}}{\gamma\,\dot{\alpha}_{motor}} \tag{11}$$

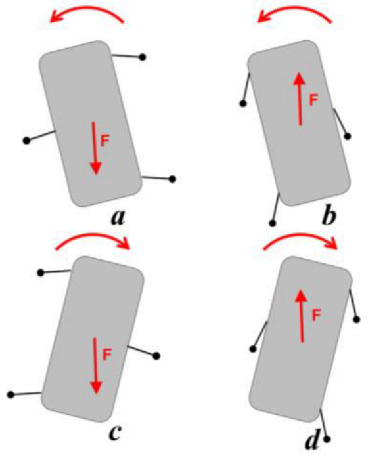

Figure 4. Yaw rotation due to an external force. Counter clockwise rotation is caused by back force on RT (a) or forward force on LT (b). Clockwise rotation is caused by either back force on LT (c) or forward force on RT (d).

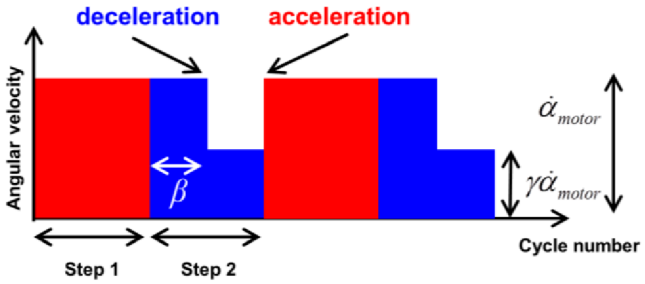

Figure 5. Input angular velocity of the motors.

D. Small perturbation analysis.

In both sections III.D and III.E, we shall estimate the maximum rotation angle, minimum radius of curvature and actuation frequency for small deformations. These approximated values allow for preliminary optimization of the design and control parameters of the robot.

When a small force δF acts on the static robot, it generates a translation δX, of the COM, and a rotation $\delta\theta$, of the body, that are proportional to its magnitude. For small δF the legs do not slide but change their orientation by $\delta\alpha$. The motion of the joints $\boldsymbol{\delta X^{(i)}}$, where i is the joint number, can be calculated as a function of the yaw rotation of the body

$$\boldsymbol{\delta X^{(i)}} = \boldsymbol{\delta} + \delta\theta\left(\hat{\mathbf{e}}_3 \times \mathbf{X_H^{(i)}}\right) \tag{12}$$

The deflections of the legs $\delta\alpha^{(i)}$ are

$$\delta\alpha^{(i)} = \pm\frac{\left(\mathbf{L^{(i)}} \times \boldsymbol{\delta X^{(i)}}\right)\cdot\hat{\mathbf{e}}_3}{L^2} \pm \delta\theta \tag{13}$$

The plus is for the left side legs and minus for the right side. The change in the length of the legs is

$$\delta L^{(i)} = \frac{\mathbf{L^{(i)}}}{L^{(i)}}\cdot\boldsymbol{\delta X^{(i)}} \tag{14}$$

The force acting on the robot on hip i is due to both springs

$$\delta\mathbf{f}^{(\mathbf{i})} = -k_l \left(\frac{\mathbf{L}^{(\mathbf{i})}}{\left(L^{(i)}\right)^2} \cdot \delta\mathbf{X}^{(\mathbf{i})} \right) \mathbf{L}^{(\mathbf{i})} + \left(\frac{\left(\mathbf{L}^{(\mathbf{i})} \times \delta\mathbf{X}^{(\mathbf{i})}\right) \cdot \hat{\mathbf{e}}_3}{\left(L^{(i)}\right)^2} + \delta\theta \right) \frac{k_r}{L^{(i)}} \mathbf{L}^{(\mathbf{i})} \times \hat{\mathbf{e}}_3 \tag{15}$$

As the robot is in equilibrium, the total sum of forces and moments is zero.

$$\sum_i \delta\mathbf{f}^{(\mathbf{i})} + \delta\mathbf{F} = 0 \tag{16}$$

and

$$\sum_i \left(\mathbf{X}_\mathbf{H}^{(\mathbf{i})} + \mathbf{L}^{(\mathbf{i})} \right) \times \delta\mathbf{f}^{(\mathbf{i})} = 0 \tag{17}$$

Solving Eqs. (16) and (17) gives the yaw rotation angle as linear function of δF

$$\delta\theta = C \cdot \delta F \tag{18}$$

the maximum acceleration value that the robot is can achieve is limited by the COF

$$\frac{\delta F}{m} \le \mu \cdot g \tag{19}$$

The maximum possible rotation relative to the COF during a cycle, comprised of two steps, is

$$\left|\delta\theta\right|_{cycle} \le 2\left|C\right| \cdot \left(\mu \cdot m \cdot g\right) \tag{20}$$

E. Radius of Rotation for small deformation

Alternatively, the turning angle, radius of rotation and center of rotation can be calculated as a function of the motion of any two points of the body of the robot. For simplicity, we choose the left and right hips of the center legs (3,4) and that the weight is divided equally between the two sides. In an RT configuration, the maximum friction force acting on a single right leg is $m \cdot g \cdot \mu /4$ and on the left leg is $m \cdot g \cdot \mu /2$. We denote by Δx_l and Δx_r, respectively, the motion of the left and right sides during a step. Their values can be approximated as

$$\Delta x_l \approx L_s \pm \frac{\mu m\ g\ L \cos\left(\alpha_{step}/2\right)}{2k_r} \tag{21}$$

$$\Delta x_r \approx L_s \pm \frac{\mu m\ g\ L \cos\left(\alpha_{step}/2\right)}{4k_r} \tag{22}$$

The plus is for LT deceleration and minus for RT acceleration. Alternatively

$$\Delta x_l = \Delta\theta \left(R - \frac{w}{2} \right) \tag{23}$$

Where $\Delta\theta$ is the rotation angle and R is the radius of rotation (see Figure 6). Similarly

$$\Delta x_r = \Delta\theta \left(R + \frac{w}{2} \right) \tag{24}$$

Subtracting Eq. (23) from Eq. (24), we obtain an explicit value of θ

$$\Delta\theta \approx \frac{\mu m\ g\ L \cos\left(\alpha_{step}/2\right)}{4wk_r} \tag{25}$$

Inserting (25) into (24) yields the radius of curvature R

$$R = \frac{w}{2} \frac{\Delta x_l + \Delta x_r}{\Delta x_r - \Delta x_l} \tag{26}$$

Inserting (21) and (22) we obtain

$$R \approx w \left(\frac{4k_r\ L_s}{\mu m\ g\ L \cos\left(\alpha_{step}/2\right)} \pm \frac{3}{2} \right) \tag{27}$$

We note that this approximation is correct for small deformations only and that the radius of rotation is larger during deceleration than it is during acceleration

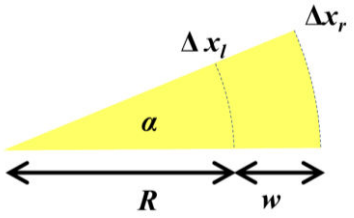

Figure 6. The rotation angle and radius of curvature.

IV. NUMERICAL SIMULATION AND COMPARISON TO ANALYSIS

A numerical simulation for the dynamic model of the robot, as per equations (6)-(9), was developed. The purpose of the simulation is first to validate the analytical predictions of steering, second to evaluate the actual velocity and radius of curvatures by using realistic parameters of previous robot designs [1][11], and third to find optimum parameters for tuning. Unless otherwise stated, the values of the simulation parameters are:

m=0.03kg,
k_l=10N/m, k_r=0.004Nm,
L_r=0.1m, L_0=0.02m, w=0.04m,
μ=0.5,
γ=0.5, β=1/3 and α_{step}=π/3.
The selected values of γ and β satisfy T_1=T_2 (11).

A. Turning counter clockwise and then clockwise

Figure 7 presents the trajectory of the robot rotating at an actuation frequency of 6Hz. The robot first completes a counterclockwise (accelerate at RT and decelerate at LT) circle and then makes a clockwise (decelerate at RT and accelerate at LT) circle.

Figure 8 and 9 present the linear and angular velocities of the robot turning counter clockwise at 6Hz. The robot reaches a stable gait after two cycles. The linear velocity varies between 0.07m/s and 0.31m/s, with an average of 0.2m/s, compared to the nominal velocity of 0.48m/s as per Eq. (4). The angular velocity alternates between 0 and 0.7

rad/s but has typically two phases, the first (and larger) is due to acceleration and the second due to deceleration. At an average rotation rate of 0.35rad/s, the robot can perform a "U turn" in roughly 9 seconds. The maximum angular velocity as per equation (20) is 0.52rad/s and the minimum radius of rotation estimated using linear model (20) and (27) is, respectively, 0.19m and 0.31m compared to 0.61m obtained from the simulation. The difference is due to the non-linear model of the robot, sliding, and to the fact that the simulated robot was unable to achieve full rotational speed, especially during the deceleration (see figure 9).

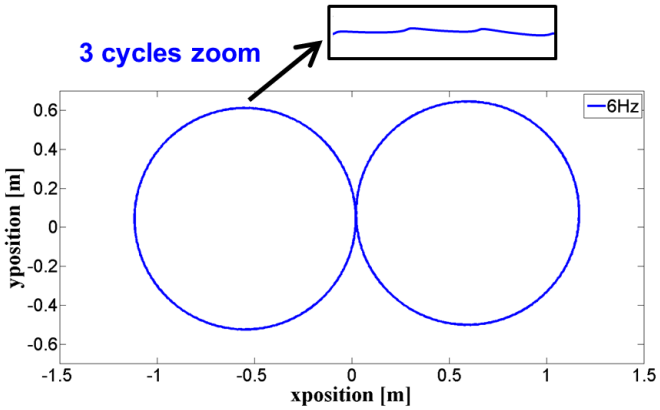

Figure 7. Trajectory of the robot turning at 6Hz and a zoom to 3 cycles.

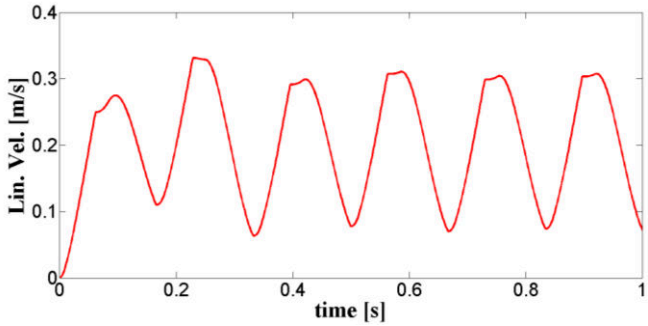

Figure 8. Linear velocity of the robot running at 6Hz.

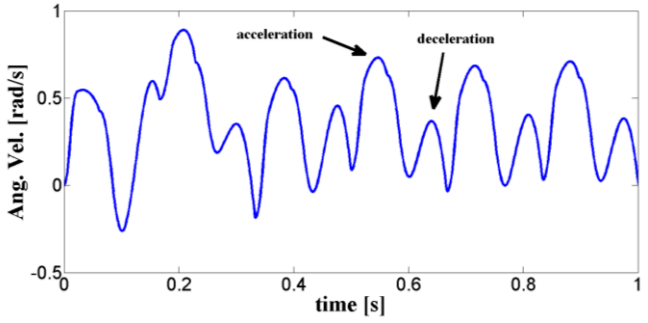

Figure 9. Angular velocity of the robot running at 6Hz. The different peaks are due to the acceleration and deceleration of the motor.

B. Minimum friction requirements

The COF depends on the contact materials of the tips of the legs and the surface. Its value typically varies between 0.2 and 0.3 for rigid-rigid contacts to beyond 1 for flexible materials such as rubber. Figure 10 presents the radius of rotation as function of the COF for three different frequencies. As the maximum acceleration and deceleration of the robot are proportional to the COF, see Eq. (19), the robot is capable of turning at low COF but the radius is larger. The radius decreases as function of the COF but little change is noticed beyond μ=0.6, as the amount of slip becomes very small. The radii were virtually the same for μ =1 and μ =10.

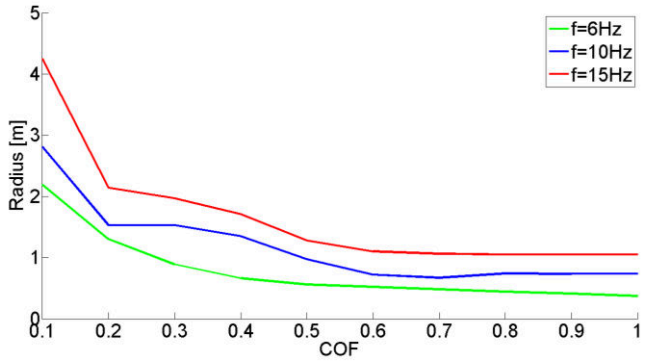

Figure 10. The radius of rotation as function of COF.

C. Gait control

The robot is controlled through the actuation frequency and the duty cycle. Figure 11 presents the radius of curvature as function of the actuation frequency for three different COF, 0.2, 0.5 and 1. The radius of curvature increases almost linearly in the range between 6Hz and 15Hz. Below 6Hz, the radius increases and becomes infinite at 4.05Hz (roughly half of the natural frequency of the robot) and turns in the opposite direction for lower frequencies.

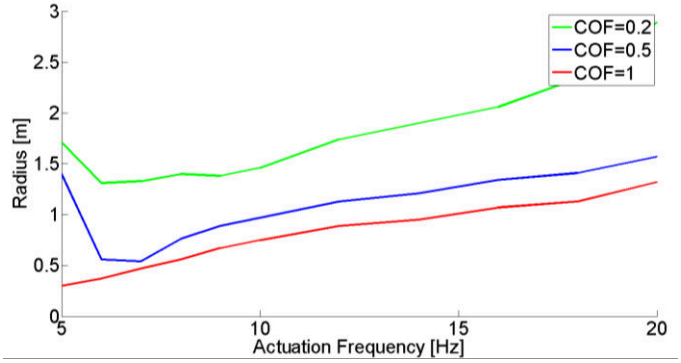

Figure 11. Radius of rotation as function of the frequency of locomotion.

The radius as function of the duty cycle β is presented in Figure 12. The minimum radius is obtained at 0.35 which yields to $T_1 \approx T_2$. Its value remains almost unchanged between 0.3 and 0.7 but increases exponentially beyond this interval.

D. Stability of locomotion

The robot's actuation consists of acceleration and deceleration at each cycle. The frequency of the introduced perturbation is twice the actuation frequency. Therefore, one should avoid actuating the robot at one half of its natural frequency, which, for the selected parameters, is roughly 7.8 Hz. At the critical frequency (4.05Hz), the robot may

become unstable and will not turn. Beyond 4.05Hz, the locomotion is stable and reaches its best performance at roughly 6Hz. Below the critical frequency, the robot may turn opposite to the desired direction as it may oscillate a multiple of time during a single step.

The input energy of the robot is dissipated by two means, sliding of the legs over the surface and dissipation of elastic energy of the linear and torsional springs during the disengagement of the legs from the surface. For high COF, little or no sliding occurs and stability is reduced. An increase of the torsional spring's stiffness reduces the yaw rotation of the robot as the robot becomes less sensitive to tilting. However, an increase in the stiffness of the linear springs, together with high COF, causes the robot to oscillate sideways at high rate and become unstable.

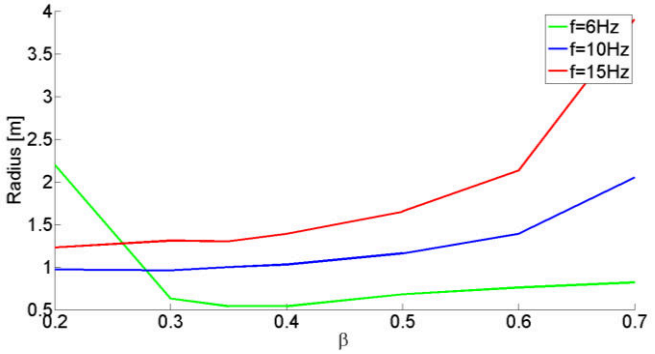

Figure 12. Radius of curvature as function of β

V. CONCLUSIONS

The research, described in the present manuscript, focused on a novel gait of actuation for hexapods which allows crawling forward, backward and turning using a single actuator. The gait exploits the stiffness difference between the two sides of the tripod to cause tilting by accelerating or decelerating the motion of the legs. Successive tilting in the same orientation causes continuous rotation of the robot in the desired direction.

The robot is modeled as a rigid body with massless but compliant legs. We used the Coulomb contact to simulate the interaction between the tips of the legs and surface. A static analysis and dynamic analyses of the robot are presented in section III. The static analysis allows us to obtain a preliminary estimate of the amount of rotation the robot will make during a cycle as a function of the compliance of the legs, the mass and the COF.

To validate our expectations, a numerical simulation was performed based on realistic robot parameters. The performance was investigated as function of the actuation frequency, COF and duty cycle. Best performance is achieved slightly above the critical frequency together with equal periods for low and high velocities. At the critical frequency, the robot does not rotate and below critical frequency, the motion becomes chaotic and the robot may turn either direction. The robot is capable of rotating with a COF as low as 0.2 but its performance improves as the COF increases up to 0.6. Beyond that, little change is noticed.

VI. REFERENCES

[1] P. Birkmeyer, K. Peterson, and R.S. Fearing, "DASH: A dynamic 16g hexapedal robot", IEEE Int. Conf. on Intelligent Robots and Systems, pp. 2683-2689, 2009.

[2] J.G Cham, S.A. Bailey, J.E. Clark, R.J. Full, and M.R. Cutkosky, "Fast and robust: Hexapedal robots via shape deposition manufacturing", *The Int. Journal of Robotics Research*, Vol. 21, no. 10-11, pp. 869-882, 2002.

[3] R. J. Full, T. Kubow, J. Schmitt, P. Holmes, and D. Koditschek, " Quantifying dynamic stability and maneuverability in legged locomotion", *Integrative and Comparative Biol.* Vol. 42, pp. 149-157, 2002.

[4] P. Holmes, R. J. Full, D. Koditschek, J. Guckenheimer, " The dynamics of legged locomotion: models, analyses and challenges", *SIAM Review*, Vol. 48, No. 2, pp. 207-304.

[5] A. M. Hoover, S. Burden, X.Y. Fu, S. S. Sastry, and R. Fearing, "Bio-inspired design and dynamic maneuverability of a minimally actuated six-legged Robot", IEEE International Conference on Biomedical Robotics and Biomechatronics, pp. 869-873, 2010.

[6] D. L. Jindrich, and R. Full, "Dynamic stabilization of raid hexapedal locomotion", *Journal of Exp. Biol.*, 205, pp. 2803-2823, 2002.

[7] R. P. Kukillaya, P. Holmes, "A hexapedal jointed-leg model for insect locomotion in the horizontal plane", *Biol. Cyber.*, DOI 10.1007/s00422-007-0180-2, 2007.

[8] S. Kim, J. E. Clark, and M. R. Cutkosky, "iSprawl: Design and turning of high-speed autonomous open-loop running", *The Int. Journal of Robotic Research*, Vol. 25, No.9. pp. 903-912, 2006.

[9] A. McClung, "Techniques for dynamic maneuvering of hexpedal legged robots," Ph.D. diss., Stanford University, 2006.

[10] J.M. Morrey, B. Lambrecht, A.D. Horchler, R. E. Ritzmann, and R.D. Quinn, " Highly modbile and robust small quadruped robots", IEEE Int. Conf. on Intelligent Robots and Systems, Vol. 1, pp. 82-87, 2003.

[11] A.O. Pullin, N. J. Kohut, D. Zarrouk, and R.S. Fearing, "Dynamic Turning of 13cm robot comparing tail and differential drive", IEEE Int. Conf. on Robotics and Automation, pp. 5083-5093, 2012.

[12] J. Schmitt, P. Holmes, "Mechanical models for insect locomotion: dynamics and stability in the horizontal plane I. Theory", *Biol. Cyber.* Vol. 83, pp. 501-515, 2000.

[13] J. Schmitt, P. Holmes, "Mechanical models for insect locomotion: dynamics and stability in the horizontal plane II. Application", *Biol. Cyber.* Vol. 83, pp. 517-527, 2000.

[14] K. Tsujita, H. Toui, and K. Tsuchiya, "Dynamic turning control of a quadruped robot using nonlinear oscillators," Proc. IEEE/RSJ Int. Conf. on Intelligent Robots and Systems, pp. 969-974, 2004.

[15] J. D. Weingarten, G. A. D. Lopes, M. Buehler, R. E. Groff, and D. E. Koditschek, "Automated gait adaptation for legged robotos", IEEE Int. Conf. on Robotics and Automation, pp. 2153-2158, 2004.

[16] D. Zarrouk, I. Sharf, and M. Shoham, "Analysis of worm-like robotics locomotion on compliant surfaces", *IEEE, Trans. on Biomedical Engineering*, Vol. 58, No. 2, pp. 301-309, 2011.

[17] D. Zarrouk, I. Sharf, M. Shoham, "Conditions for worm-robot locomotion in flexible environment: Theory and Experiments. *IEEE Trans. on Biomedical Engineering*, Vol. 59, No. 4, pp. 1057-1067, 2012.